



ELSEVIER

Earth and Planetary Science Letters 156 (1998) 239–252

EPSL

# Gravity anomalies and segmentation of the continental margin offshore West Africa

A.B. Watts\*, J. Stewart

*Department of Earth Sciences, Parks Road, Oxford OX1 3PR, UK*

Received 15 September 1997; revised version received 12 January 1998; accepted 16 January 1998

## Abstract

The free-air gravity 'edge effect' anomaly at passive continental margins provides constraints on the thermal and mechanical properties of the lithosphere in extensional regions. Like many margins, the edge effect 'high' offshore Gabon, West Africa is located at the shelf break in the region of maximum sediment thickness. Gabon differs, however, from other margins in that the edge effect 'low' is displaced from over the continental rise to the slope. The origin of the low has been investigated by backstripping the sediments at the margin. We have used the backstrip to calculate the amount of crustal thinning, assuming Airy isostasy. Such a model implies zero strength during rifting. Alternatively, this amount of crustal thinning can be explained by a strong margin and a depth of necking that exactly balances the upward and downward forces that act on the crust during rifting. We have developed a method, which takes into account variations in the strength during rifting and the depth of necking, to compute the thinning *directly* from the sediment backstrip. The backstrip and the crustal thinning have been used to calculate the rifting gravity anomaly. Differences between the backstrip and the present-day water depth give the geometry of the sediment load and hence, the contribution to the gravity anomaly of sedimentation. By comparing the *combined* rifting and sedimentation anomaly to the observed free-air gravity anomaly, we have been able to constrain the flexural rigidity (and equivalent elastic thickness,  $T_e$ ) of the lithosphere during and after rifting. The best fitting model is one in which the 'low' is caused by a 125 km wide zone of relatively thin (i.e. ~15 km) continental crust which was weak (i.e.  $0 < T_e < 10$  km) during rifting and has remained so since then. We speculate that the weak zone extends for 350–400 km *along-strike* of the Gabon margin and that passive margins may be highly segmented as regards their long-term strength. © 1998 Elsevier Science B.V. All rights reserved.

*Keywords:* gravity anomalies; flexure; continental margin

## 1. Introduction

Passive continental margins form in response to continental rifting and the creation of new ocean basins. Some margins are characterised by relatively thin sediments and either an absence (e.g. Goban

Spur [1]) or abundance (e.g. Vøring [2]) of magmatic material. Evidence for magmatism occurs either in the form of seaward dipping reflector sequences or high P-wave velocity (i.e.  $>7.3$  km s<sup>-1</sup>) underplated lower crustal bodies or some combination of these features. Others (e.g. East Coast, USA) correlate with large thicknesses of sediments ( $>10$  km) which make it difficult to evaluate the role of magmatism. While differences in the amounts of sediments

\* Corresponding author. Fax: +44 (1865) 272-2032; E-mail: tony@earth.ox.ac.uk

and magmatism explain the diversity of present-day margins, they obscure the geometry, styles and mechanics of initial rifting.

One approach to the problem is to develop better seismic techniques to image the deep crustal structure of passive margins. Unfortunately, it has proved difficult to use seismic reflection and refraction data to resolve issues such as the presence or absence of detachment surfaces and the style of rifting at margins, despite major advances in data acquisition techniques. Multiples generated from within the sedimentary column and penetration beneath basaltic sill complexes are two of the problems that need to be overcome in the future in order to better understand the deep structure of these features.

Another approach is by backstripping [3]. This is a quantitative technique which allows the contribution of sediment loading and underplating to be evaluated and the crustal structure produced by rifting to be isolated. Such calculations are dependent, however, on a number of parameters. These include the long-term (i.e.  $>10^6$  a) flexural strength of extended continental lithosphere. Some constraints can be placed, however, on the strength by comparing the observed gravity anomaly to calculations of the combined gravity effect of the crustal structure due to rifting and other processes such as sedimentation and underplating.

Combined backstripping and gravity modelling studies offshore the East Coast, USA [4] suggest that sediments there have loaded stretched continental crust which has a low flexural rigidity. A similar result was deduced by Fowler and McKenzie [5] at the Rockall and Exmouth Plateau margins. However, other margins offshore New Zealand [6], the Gulf of Lion [7] and Tyrrhenian Sea [8] are associated with high flexural rigidity. Around Africa, Watts and Marr [9] argued that there were cases where weak segments of margins abutted strong ones. Thus, whether extended crust is weak or strong is controversial.

Braun and Beaumont [10] pointed out that the response of the lithosphere to extension is a rheological problem. They suggest, based on yield strength envelope considerations [11], that thinning of the lithosphere occurs around the level of maximum strength. This level, which they define as the 'depth of necking', determines the initial configuration of the extended crust. Depending on the depth of necking there will be either a net downward or upward acting force

which attempts to restore the initial configuration to a state of isostatic equilibrium. If the crust has no strength then there will be no resistance and the adjustment of the initial basin and mantle uplift that results from extension will be the same as that predicted by an Airy model. However, if there is strength during extension then the restoring forces will be distributed flexurally, the adjustment will be limited and, significant departures may exist from an Airy model.

Although the assumption of Airy isostasy during rifting may be justified by higher lithospheric temperatures and widespread normal faulting, it seems unlikely that *all* margins will show such fundamental weakness at the time of rifting. Bertotti et al. [12], for example, have argued from field-derived data on fault timing and displacement in the southern Alps that the lithosphere preserves substantial strength prior to continental break-up and becomes stronger thereafter. Many present-day margins, despite different rifting ages, are flanked by rim uplifts which appear to require a high flexural rigidity [13]. Moreover, Kooi et al. [7], and more recently Keen and Dehler [14], have argued that inclusion of lithospheric strength during rifting is required to explain free-air gravity anomaly data at some North Atlantic margins.

The purpose of this paper is to investigate the effects of variations in strength and depth of necking during rifting at the continental margin offshore Gabon, West Africa. We chose Gabon because it is a relatively poorly explored margin and previous studies [15] indicate that it is associated with an unusual pattern of free-air gravity anomalies. We show how a *single* seismic reflection and gravity anomaly profile can be used to constrain the spatial distribution and long-term mechanical properties of extended continental lithosphere at the margin. The main conclusion that we draw is that despite their morphological linearity, the lithosphere that underlies some passive margin basins is highly segmented as regards its long-term strength.

## 2. The Gabon margin

The continental margin offshore Gabon (Fig. 1) formed by the rifting apart of South America and Africa during the Late Jurassic and Early Cretaceous. Plate kinematic studies suggest an early opening pole

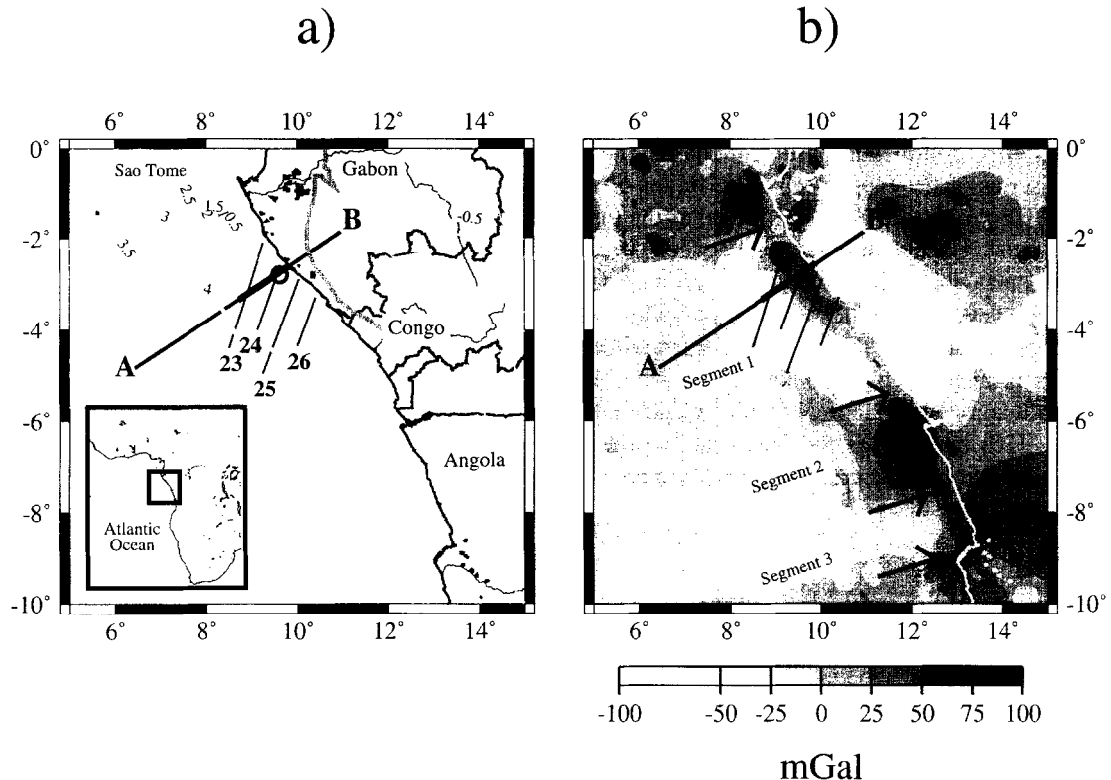


Fig. 1. Location map of the West Africa continental margin offshore Gabon, Congo and Angola. Heavy line shows the location of profile A–B. Fine lines show the location of the PROBE seismic reflection profiles lines 23–36 [19]. (a) Topography (contour interval  $-0.5$  km). Thick grey line offshore that crosses the southwest end of PROBE lines 23 and 25 indicates the ocean–continent boundary according to Meyers et al. [19]. Thick grey line onshore indicates the boundary between the Mesozoic–Tertiary rift-related sediments and Precambrian basement rocks. (b) Free-air gravity anomaly map. Thick white line offshore corresponds to the thick grey line offshore in (a). The map is based on  $2.5 \times 2.5$  minute smoothed values of all available government, academic and commercial data and was compiled by University of Leeds based company GETECH as part of its African Gravity Project [34]. Light regions show negative anomalies, dark regions positive anomalies. The significance of Segments 1, 2 and 3 is discussed in the text.

that was located near the Salvador, Brazil–Gabon coastlines [16]. The motion of Africa with respect to South America about this pole was anticlockwise and in the Gabon region, the opening direction is approximately NE–SW. The plate motion caused a progressive, south-to-north, opening of the South Atlantic rift system and rifting was coeval with the development of sinistral strike-slip faults in Central Africa and South America.

Geological studies of syn-rift basins onshore Gabon [17] and Brazil [18] suggest that rifting began in the Neocomian (i.e.  $\sim 133$  Ma) and lasted some 20 Ma. Following rifting, locally, fault-controlled, subsidence was replaced by a more basin-wide thermal subsidence. This led to the deposition of transgressive siliciclastic units which unconformably

overlie the syn-rift sediments. Extensive evaporites were also deposited along both margins prior to the formation of oceanic crust. As oceanic crust was formed and the basin widened, clastic sediments and shallow-water carbonates were deposited above the evaporites. Deposition continued from the Albian to Recent. Erosion due to corrosive bottom counter currents, however, has removed much of the Late Eocene to Oligocene deposits. By the Miocene, the rate of tectonic subsidence had slowed sufficiently on the Gabon margin for deltas to begin to prograde across the slope and rise, probably due to the lack of accommodation space on the shelf.

The only previously published constraints on the spatial distribution of rifted crust offshore Gabon are based on seismic reflection profile and magnetic

anomaly data. Meyers et al. [19], for example, identified a series of triangular block-like structures on the PROBE seismic reflection profiles which they interpret as a series of synthetic fault blocks composed of thinned continental basement rocks. They interpret a series of flat-topped reflectors on the SW end of PROBE profiles 23 and 26 (Fig. 1a) as the top of oceanic crust. The actual transition between rifted continental crust and oceanic crust was difficult to determine, however, from the seismic data. Meyers et al. [19] point out that the transition inferred on the profiles is located about 15 km landward of a large-amplitude magnetic anomaly which Cande and Rabinowitz [20] interpret as the boundary between highly magnetised oceanic crust and weakly magnetised continental crust.

### 3. Backstripping and gravity modelling

Watts [4] developed a method based on backstripping and gravity modelling to use seismic reflection profile data to determine the crustal-type beneath rifted margins. The method is based on evidence from flexure studies that continental and oceanic lithosphere respond to long-term loads in fundamentally different ways. For example, it is known from mid-oceanic ridge, oceanic island and seamount and, deep-sea trench–outer rise studies that the elastic thickness of the oceanic lithosphere,  $T_e$ , increases with age of the lithosphere *at the time of loading*. Although Karner et al. [21] suggested that continental lithosphere shows a similar dependence with age, it is difficult to explain continental  $T_e$  values by a single set of thermal parameters as is the case for the oceans. A majority of continental values, especially those from extended regions, are relatively low and in the range  $0 < T_e < 20$  km [5,22,23]. Only in the cool cratonic interiors does the continental lithosphere appear capable of showing any degree of long-term strength.

We have used high-quality seismic reflection profile data acquired by GECO during 1988 to determine the type of crust that underlies the West Africa margin, offshore Gabon. Unfortunately, it is not possible to show the original seismic data since these data still have a commercial value. However, the GECO profile crosses PROBE profiles 23 and

Table 1

Summary of parameters used in the backstripping and gravity modelling

---

$\rho_c$ = density of crust = 2800 kg m <sup>-3</sup>
$\rho_m$ = density of mantle = 3330 kg m <sup>-3</sup>
$\rho_s$ = average density of sediments (for gravity calculation) = 2350 kg m <sup>-3</sup>
$\rho_{\text{unit1}}$ = density of Unit 1 (base Miocene–Recent) = 2100 kg m <sup>-3</sup>
$\rho_{\text{unit2}}$ = density of Unit 2 (top Albian–base Miocene) = 2200 kg m <sup>-3</sup>
$\rho_{\text{unit3}}$ = density of Unit 3 (top salt–top Albian) = 2280 kg m <sup>-3</sup>
$\rho_{\text{unit4}}$ = density of Unit 4 (top rift–top salt) = 2420 kg m <sup>-3</sup>
$\rho_{\text{unit5}}$ = density of Unit 5 (top early rift–top rift) = 2500 kg m <sup>-3</sup>
$\rho_{\text{unit6}}$ = density of Unit 6 (basement–top early rift) = 2600 kg m <sup>-3</sup>
$E$ = Young's modulus = 100 GPa
$\rho$ = Poisson's ratio = 0.25
$g$ = average gravity = 9.81 m s <sup>-2</sup>

---

24 (Fig. 1) which have been published in original form [19]. We have used in this study a stratigraphic interpretation of the GECO profile that was carried out by A.D. Edwards of Fairway Geophysical. He used seismic sequence stratigraphic techniques [24] to sub-divide the profile into six 'megasequences'. The age of the four youngest units were assigned on the basis of ties with the CMB-1 well [19]. The age of the two older units were assigned on the basis of the known rifting history of the region. Finally, thicknesses were obtained from depth-converted seismic reflection profiles.

Each unit identified on the seismic reflection profile was flexurally backstripped using a density that was inferred from the seismically derived stacking and interval velocities (Table 1). The individual backstrips from each unit were then summed to obtain the depth (or elevation) that the crystalline basement that underlies the sediments would have been in the absence of sediment loads. This depth was added to the present-day water depth (i.e. the unfilled portion of the margin) to yield  $Y$ , the total tectonic subsidence and uplift at the margin. Finally, the amount of crustal thinning,  $\beta$ , required to explain  $Y$  was computed assuming Airy isostasy from:

$$\beta = \frac{t_c(\rho_m - \rho_c)}{t_c(\rho_m - \rho_c) - Y(\rho_m - \rho_w)} \quad (1)$$

where  $t_c$  is the initial crustal thickness and  $\rho_m$ ,  $\rho_c$  and

$\rho_w$  are the densities of the mantle, crust, and water, respectively (Table 1).

The first step in the modelling is to use  $\beta$  from Eq. 1 to calculate the gravity anomaly associated with rifting. The next step is to use the difference between  $Y$  and the present-day water depth to estimate the sediment load that has been added to the margin since rifting. The difference between  $Y$  and the present-day basement gives the amount of flexure due to the sediment load. The gravity anomaly associated with sedimentation is then computed from the sum of the positive contribution due to the sediment load and a negative contribution from the flexure of the basement and the underlying Moho. The final step is to combine the rifting and sedimentation anomaly to give the sum anomaly which can be compared to the observed free-air gravity anomaly.

Fig. 2 shows the rifting, sedimentation and sum gravity anomalies that were calculated after flexurally backstripping sediments at the Gabon margin with uniform  $T_e$  values of 5, 20 and 35 km. The calculated gravity anomalies show a ‘high’ over the sediment load which is flanked by ‘lows’. The highs reflect the magnitude of the sediment load while the lows are indicative of the degree to which the load is compensated. The  $T_e = 5$  km case, which corresponds to a mechanically weak crust, yields gravity anomalies that are of relatively low-amplitude and short-wavelength compared to the observed whereas the stronger  $T_e = 35$  km case yields anomalies that are of large-amplitude and long-wavelength. As would be expected, all three cases in Fig. 2 reveal a broad high with a seaward gradient that is located over the mid-point of the continental slope. This contrasts with the observed profile which shows a narrow high with a seaward gradient which is displaced landward over the upper part of the slope. Hence, none of the calculated gravity anomaly profiles in Fig. 2 adequately describe the observed data.

#### 4. The depth of necking and strength during rifting

One problem with the calculations in Fig. 2 is that they are based on the assumption of Airy isostasy during rifting. Several authors have pointed out that the crustal thinning produced by extension is not

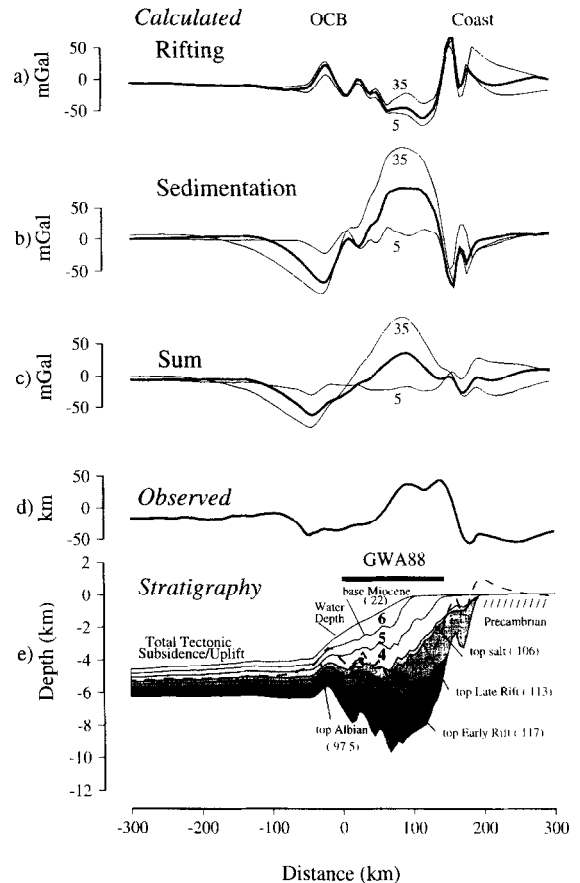


Fig. 2. Comparison of observed and calculated gravity anomalies along profile A–B (see Fig. 1 for location) of the West Africa margin, offshore Gabon. The vertical dashed lines show the location of the ocean–continent boundary according to Meyers et al. [19] and the present-day coastline. (a) Rifting anomaly based on a sediment backstrip with  $T_e = 5$  and 35 km (fine lines) and  $T_e = 20$  km (thick line). (b) Sedimentation anomaly. (c) Sum anomaly. (d) Gravity anomaly (free-air onshore, Bouguer onshore profile based on GETECH data. Grey dots show the location of the  $2.5 \times 2.5$  minute smoothed gravity anomaly values located within 15 km of the profile. Note that while the amplitude of the high and the flanking low on the seaward side are well controlled by the data, the seaward gradient of the high is not. The gradient has been verified, however, using satellite-derived gravity anomaly data. (e) Stratigraphic data based on an interpretation of the GECO-owned GWA88 seismic reflection profile by A.D. Edwards of Fairway Geophysical. The numbers in brackets give the approximate age in Ma of the horizons that defines each unit. The dashed line indicates the tectonic subsidence and uplift at the margin based on a sediment backstrip with  $T_e = 20$  km.

necessarily that predicted by an Airy-type model. An alternative model, which allows for variations in strength and depth of necking during rifting has been proposed by Braun and Beaumont [10].

Using these concepts, Weissel and Karner [13] showed that the depth of the basin depression,  $S_t$ , which would result from extension is related to the depth of necking,  $Z_{\text{neck}}$ , by:

$$S_t = \left(1 - \frac{1}{\beta}\right) Z_{\text{neck}} \quad (2)$$

The force,  $q_{\text{net}}$ , that attempts to return this depression to a state of isostatic balance is given by the sum of all the density contrasts within the lithosphere (which includes the crust), compared to that of undeformed lithosphere. These include an upward force,  $q_{\text{up}}$ , due to replacement of crust by water and a downward force,  $q_{\text{down}}$ , due to replacement of crust by mantle. Ignoring the thermal effects on the density of the sub-crustal mantle, we get:

$$q_{\text{net}} = q_{\text{up}} + q_{\text{down}} \quad (3)$$

$$q_{\text{net}} = (S_t \Delta \rho_1 + S_m \Delta \rho_2) g$$

where  $\Delta \rho_1 = (\rho_w - \rho_c)$ ,  $\Delta \rho_2 = (\rho_m - \rho_c)$ ,  $S_m$  is the Moho upwarp, and  $g$  is average gravity.

The deformation associated with  $q_{\text{net}}$  will be distributed according to the strength of the lithosphere during rifting. If the lithosphere has no strength then the restoring forces will return the depression to a state of Airy-type isostatic equilibrium, with a final depression of the basin,  $Y$ , obtained simply by rearranging Eq. 1:

$$Y = t_c \left(1 - \frac{1}{\beta}\right) \frac{\rho_m - \rho_c}{\rho_m - \rho_w} \quad (4)$$

If, on the other hand, there is strength during rifting then the shape of a basin will be modified by flexure. As shown in Fig. 3, the initial depression,  $S_t$ , depends critically on  $Z_{\text{neck}}$ . For a shallow  $Z_{\text{neck}}$  (Fig. 3a) the depth of the basin is small in comparison to the magnitude of the Moho upwarp and a downward state of flexure results, predicting basin margin subsidence, relative to the Airy case. For deep depths (Fig. 3c) an upward state of flexure prevails, predicting an upwarp in the basin centre and uplift on the basin flanks relative to the Airy case. For one particular  $Z_{\text{neck}}$  (Fig. 3b) the upward

and downward forces exactly balance, and the final basin shape is the same as the initial configuration.

The final position of the basin after taking into account  $Z_{\text{neck}}$  and flexure is the position that basement would be in the absence of sediment loads. This is also the depth that would be obtained from backstripping,  $Y$ . We therefore require an expression that uses the observable  $Y$  to determine the amount of crustal thinning *and* takes into account  $Z_{\text{neck}}$  and the strength of the lithosphere during rifting.

We have from combining Eqs. 2 and 3 that

$$q_{\text{net}} = \left[ S_t (\Delta \rho_1 - \Delta \rho_2) + \left(1 - \frac{1}{\beta}\right) t_c \Delta \rho_2 \right] g$$

$$= \left[ \left(1 - \frac{1}{\beta}\right) Z_{\text{neck}} \Delta \rho_3 + \left(1 - \frac{1}{\beta}\right) t_c \Delta \rho_2 \right] g$$

$$= \left( Z_{\text{neck}} \Delta \rho_3 + t_c \Delta \rho_2 - \frac{Z_{\text{neck}} \Delta \rho_3 + t_c \Delta \rho_2}{\beta} \right) g$$

$$= q_0 \left(1 - \frac{1}{\beta}\right)$$

where  $\Delta \rho_3 = \rho_w - \rho_m$  and  $q_0 = (Z_{\text{neck}} \Delta \rho_3 + t_c \Delta \rho_2) g = q_0 - q_0 \beta^{-1}$ .

For the parameters in Table 1, we see that  $q_{\text{net}} = 0$  if  $Z_{\text{neck}} = 7.2$  km. Necking at this specific depth will therefore give a final basin geometry identical to that predicted by the Airy model, despite the possibility that the lithosphere may possess strength during rifting.

The flexure of the lithosphere,  $w$ , that results from the load  $q_{\text{net}}$  is obtained from the solution of the elastic plate equation, i.e.

$$D \frac{d^4 w}{dx^4} + (\rho_m - \rho_w) w g = q_0 - q_0 \beta^{-1} \quad (5)$$

where  $D$  is the flexural rigidity during rifting. The flexural rigidity is determined from the elastic thickness,  $T_e$ , during rifting by:

$$D = \frac{E T_e^3}{12(1 - \sigma^2)}$$

where  $E$  = Young's modulus and  $\sigma$  is Poisson's ratio. The solution to Eq. 5 can be obtained by taking the Fourier Transform of both sides:

$$\mathbf{W}(k) [Dk^4 + (\rho_m - \rho_w)g] = \mathbf{Q}_0(k) - q_0 \beta^{-1}(k)$$

$$\mathbf{W}(k) \Phi(k) = \mathbf{Q}_0(k) - q_0 \beta^{-1}(k) \quad (6)$$

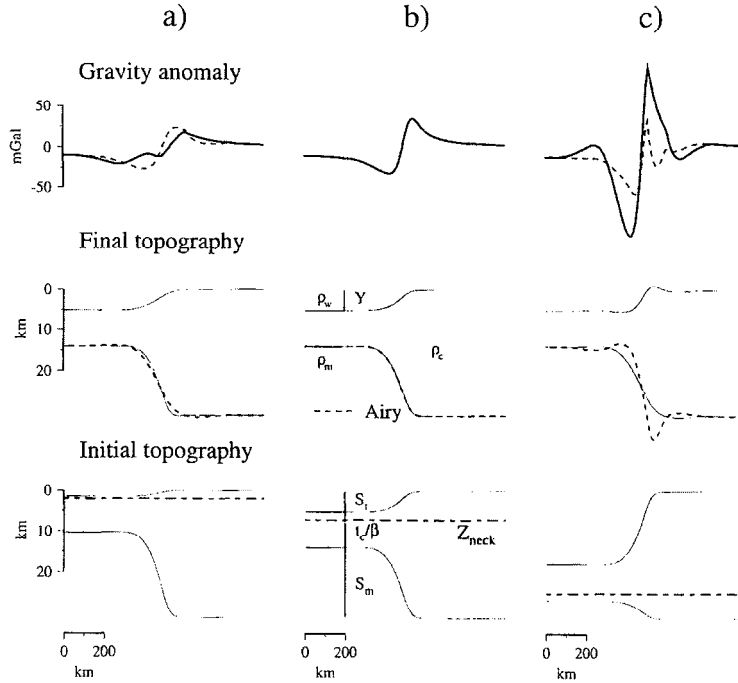


Fig. 3. The relationship between  $Z_{\text{neck}}$ ,  $S_t$ ,  $S_m$  and  $Y$  for a theoretical continental margin based on a  $T_e$  during rifting = 25 km. The top panel shows the gravity anomaly (free-air offshore, Bouguer onshore) associated with the margin structure (solid lines) in the middle panel. The dashed lines show the gravity anomalies and Moho configuration that would be predicted by an Airy model, except in the gravity anomaly in (b) where the curves are superimposed. (a)  $Z_{\text{neck}} = 2$  km. In this case, there is an initial net downward force that acts on the extended crust. The extended crust tries to isostatically adjust to these forces but, because of the finite strength of the lithosphere the final basin, Moho configuration and gravity anomaly do not correspond to the Airy case (dashed lines). (b)  $Z_{\text{neck}} = 7.2$  km. In this case, there is a balance in the forces associated with extension such that the final basin, Moho configuration and gravity anomaly is the same as would be predicted by an Airy-type model. (c)  $Z_{\text{neck}} = 25$  km. In this case, there is an initial net upward force. Again, the extended crust tries to adjust locally but, is prevented from doing so by the strength of the lithosphere. This case shows the largest departures from the Airy case with the depth to Moho being deeper and gravity anomaly 'low' more negative over the slope and, the depth to Moho being shallower and the gravity anomaly 'high' more positive in the region of the shelf break.

where the bold upper case variable represents the Fourier Transform of the lower case variable and  $\Phi(k) = Dk^4 + (\rho_m - \rho_w)g$ .

We note that  $w$  is the response of the lithosphere to the downward or upward acting loads and so is the difference between the final basin shape,  $Y$ , and the initial basin depression,  $S_t$

$$\begin{aligned}
 w &= Y - S_t \\
 &= (Y - Z_{\text{neck}}) - (S_t - Z_{\text{neck}}) \\
 &= (Y - Z_{\text{neck}}) - \left[ \left(1 - \frac{1}{\beta}\right) Z_{\text{neck}} - Z_{\text{neck}} \right] \\
 &= (Y - Z_{\text{neck}}) + Z_{\text{neck}}\beta^{-1} \\
 &= Y^* + Z_{\text{neck}}\beta^{-1}
 \end{aligned} \tag{7}$$

where  $Y^* = Y - Z_{\text{neck}}$ . Taking the Fourier Transform of both sides of Eq. 7 and equating with Eq. 6 yields:

$$\begin{aligned}
 (\mathbf{Y}^*(k) + Z_{\text{neck}}\beta^{-1})\Phi(k) &= \mathbf{Q}_0 - q_0\beta^{-1} \\
 \therefore \beta &= \frac{Z_{\text{neck}}\Phi(k) + q_0}{\mathbf{Q}_0(k) - \mathbf{Y}^*(k)\Phi(k)}
 \end{aligned} \tag{8}$$

The usefulness of Eq. 8 is that it allows the  $\beta$  distribution to be determined *directly* from a back-stripped profile  $Y$  taking into account the possibility of strength during rifting and  $Z_{\text{neck}}$ . Once  $\beta$  is determined, then it is a simple matter to compute the Moho configuration and, hence, the rifting gravity anomaly.

## 5. Results

We show in Fig. 4 the sum gravity anomaly that would be expected for different  $T_e$  during rifting and  $Z_{neck}$ . The vertical columns show the results based on sediment backstripping with a  $T_e$  (sediment) (i.e. the elastic thickness of the lithosphere that is loaded by sediment after rifting) of 5 (Fig. 4a), 20 (Fig. 4b) and 35 km (Fig. 4c). In each column, the *same* backstrip is used to calculate the crustal structure due to rifting: the different curves showing the effects of differences in  $T_e$  during rifting and  $Z_{neck}$ . Because the backstrip is the same in each column, the sedimentation anomaly will also be the same. The sum anomalies therefore directly reflect the contribution to the gravity anomaly of differences in  $T_e$  during rifting and  $Z_{neck}$ .

Fig. 4 shows that increasing  $T_e$  during rifting either *decreases* or *increases* the amplitude of the edge effect high. If  $Z_{neck} > 7.2$  km a net upward

force acts on the crust (e.g. Fig. 3c) and, depending on the  $T_e$  during rifting, there will be a relative uplift in the basin centre and flanking regions. If  $T_e$  during rifting is low there is little resistance and the uplift approaches that expected for an Airy model. The sum anomalies therefore resemble the Airy case. However, if  $T_e$  during rifting is large there is resistance such that the uplift is broad and of low amplitude. The water-filled basin is therefore not as shallow as the low  $T_e$  case would predict and there will be a greater contribution from the water and, hence, small-amplitude sum anomalies. This is seen in the top four profiles of Fig. 4a,b which show the sum anomalies corresponding to  $Z_{neck} = 10$  km and  $T_e$  during rifting in the range 0–50 km. The opposite effect occurs for  $Z_{neck} < 7.2$  km when a net downward force prevails (e.g. Fig. 3a). With a high  $T_e$  during rifting the basin is not as deep as the low  $T_e$  case would predict and there will be a smaller contribution from the water, a larger one from the

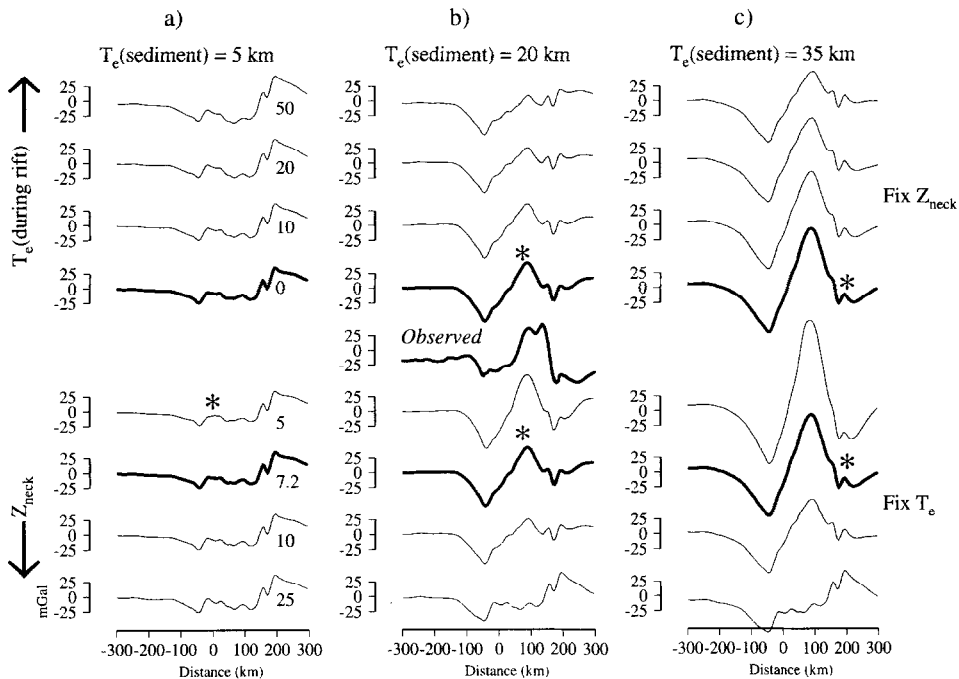


Fig. 4. Comparison of observed gravity anomalies to the predictions of models based on different  $T_e$  during and after rifting and  $Z_{neck}$ . The figure shows the results for a sediment backstrip with different values of  $T_e$  associated with the sediments that accumulate after rifting: (a)  $T_e$  (sediment) = 5 km, (b)  $T_e$  (sediment) = 20 km, and (c)  $T_e$  (sediment) = 35 km. Within each backstrip case, the top four profiles show the effect on the sum anomaly of fixing  $Z_{neck} = 10$  km and varying  $T_e$  (during rifting) from 0 to 50 km. The bottom four profiles show the effect of setting  $T_e$  during rifting to be the same as  $T_e$  (sediment) and varying  $Z_{neck}$  from 5 to 25 km. The heavy lined calculated profiles in each backstrip are identical for the reasons explained in the text. The vertical dashed lines are as in Fig. 2. The asterisks show those portions of the calculated profiles which are particularly well explained by the observed data.

mantle and, large-amplitude sum anomalies. This is most clearly seen in the fifth profile from the top in Fig. 4c which shows that when  $Z_{\text{neck}} = 5$  km and  $T_e$  during rifting = 35 km, the sum anomaly is of larger amplitude than would be predicted by an Airy model.

In the same way that increases in  $T_e$  during rifting depend on  $Z_{\text{neck}}$ , so does the effect of changing  $Z_{\text{neck}}$  depend on  $T_e$ . Except for low  $T_e$ , when  $Z_{\text{neck}}$  has little effect on the sum anomalies since the final basin shape is similar to the Airy case, the effect of increasing  $Z_{\text{neck}}$  is to decrease the amplitude of the sum anomalies. This is because  $Z_{\text{neck}}$  determines the initial depth of the water-filled depression. When  $Z_{\text{neck}}$  is small there is both a shallow basin and a net downward force. If flexure is important then the basin may be too shallow (compared to the Airy case) and the sum anomalies will be dominated by the mantle effect. When  $Z_{\text{neck}}$  is large there is both a deep basin and a net upward force. Again, if flexure is important then the basin may, in this case, be too deep and the sum anomalies will be dominated by the water effect.

Although the calculated profiles in Fig. 4 are based on backstripping and different values of  $T_e$  during and after rifting and  $Z_{\text{neck}}$ , few of them resemble the shape of the observed free-air gravity edge effect anomaly. However, a closer inspection reveals that there are features of the calculated profiles which do represent the observed data quite well. For example, the seaward low suggests that irrespective of the  $T_e$  during rifting and  $Z_{\text{neck}}$ ,  $5 < T_e$  (sediment)  $< 20$  km. The lower end of the range (which predicts a similar anomaly pattern as the  $Z_{\text{neck}} = 7.2$  km case) is preferred because it predicts the 'flattest' low. Certainly, it would be difficult to explain the low with  $T_e$  (sediment)  $\geq 20$  km unless  $T_e$  during rifting or  $Z_{\text{neck}}$  were very high. The edge effect high, however, suggests a  $T_e$  (sediment)  $\sim 20$  km with either a low  $T_e$  during rifting, or a high  $T_e$  with  $Z_{\text{neck}} = 7.2$  km. Again, a higher  $T_e$  (sediment) is possible but, only if the  $T_e$  during rifting and  $Z_{\text{neck}}$  are very high. Finally, the landward low appears to require  $T_e$  (sediment) of 35 km, or higher, with either a high  $T_e$  during rifting, or a low  $T_e$  with  $Z_{\text{neck}} = 7.2$  km.

The comparison of observed and calculated sum anomalies in Fig. 4 suggests a model in which  $T_e$

(sediment) varies spatially across the margin, from low values over the continental slope to higher ones over the shelf, and  $Z_{\text{neck}} = 7.2$  km. Since necking at this depth gives a basin shape that approximates the Airy model, it is entirely plausible that the  $T_e$  during rifting is the same as that following rifting. We cannot rule out the possibility, however, that  $T_e \geq 0$  during rifting in the weak zone since  $Z_{\text{neck}} = 7.2$  km.

We have therefore constructed a model that takes into account spatial changes in  $T_e$  across a margin. The model uses the finite difference method [25] to backstrip the sediments and obtain  $Y$ .  $\beta$  was then estimated from  $Y$  using a modified version of Eq. 8 [26], which takes into account the possibility of spatial changes in  $T_e$  during rifting.

The results of the calculations are shown in Fig. 5. The heavy solid line is the best overall fit to the observed data and was computed for an average sediment density,  $\rho_s$ , of  $2350 \text{ kg m}^{-3}$ ,  $Z_{\text{neck}} = 7.2$  km and, the  $T_e$  distribution of Model 1 which includes a weak zone. The calculated profile explains the main features of the observed profile. In particular, it explains the overall shape of the observed low and the amplitude of the flanking high. The calculated profile also explains the gradient of the seaward edge of the high as well as its location over the uppermost part of the continental slope.

The main discrepancy between observed and calculated profiles is in the region of the landward gradient of the gravity high. Although the calculated sum anomaly predicts a gravity anomaly high which correlates with a region of relatively shallow basement, the high is of smaller amplitude than is observed. We believe therefore that the high is unrelated to rifting and sediment loading and most likely results from a relatively dense body in the underlying basement.

Fig. 5 shows the sensitivity of the calculated profile to changes in  $\rho_s$ ,  $Z_{\text{neck}}$  and  $T_e$ . Changes in  $\rho_s$  (Fig. 5c) influence the amplitude of the calculated high. However,  $\rho_s = 2450 \text{ kg m}^{-3}$  appears too high while  $\rho_s = 2250 \text{ kg m}^{-3}$  appears too low. Changing  $Z_{\text{neck}}$  (Fig. 5b) has no effect on the low on the seaward side of the high. The main effect of  $Z_{\text{neck}}$  is to change the amplitude of the high and the low that flanks it on the landward side. As would be expected from Fig. 4, increasing  $Z_{\text{neck}}$  decreases

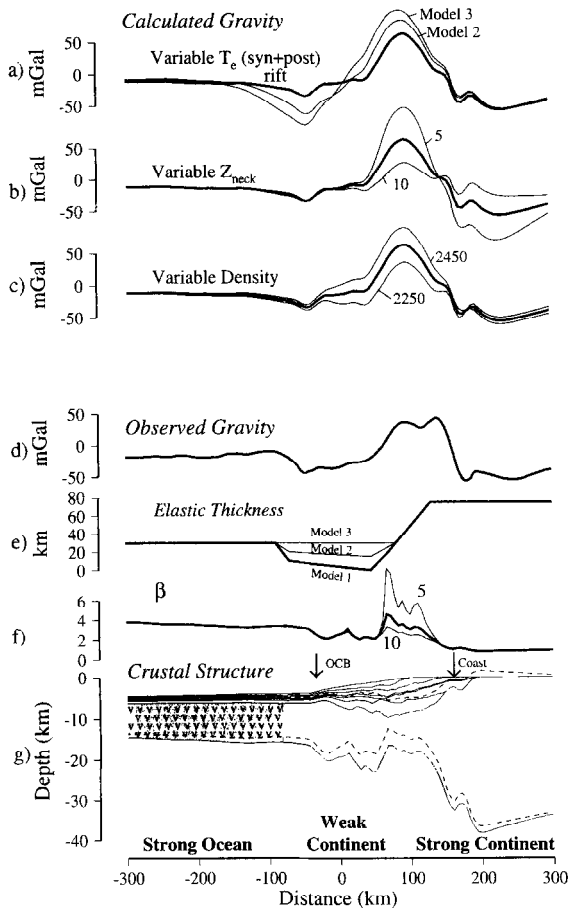


Fig. 5. Comparison of observed gravity anomalies to the calculations based on a spatially varying  $T_e$  during and after rifting. (a) Calculated anomaly based on different models for the  $T_e$  structure and the best fitting values of  $\rho_s = 2350 \text{ kg m}^{-3}$  and  $Z_{\text{neck}} = 7.2 \text{ km}$ . Model 1 (heavy lined profile) incorporates a weak zone, Model 2 is an intermediate case and Model 3 has no weak zone. (b) Calculated anomaly based on Model 1,  $\rho_s = 2350 \text{ kg m}^{-3}$  and variable  $Z_{\text{neck}}$ . Heavy lined profile based on  $Z_{\text{neck}} = 7.2 \text{ km}$ . Fine lined profiles based on  $Z_{\text{neck}} = 5$  and  $10 \text{ km}$ . (c) Calculated anomaly based on Model 1 and  $Z_{\text{neck}} = 7.2 \text{ km}$  and variable  $\rho_s$ . Heavy line based on  $\rho_s = 2350 \text{ kg m}^{-3}$ . Fine lined profiles based on  $\rho_s = 2250$  and  $2450 \text{ kg m}^{-3}$ . (d) Observed gravity anomaly. (e)  $T_e$  during and after rifting for Models 1, 2 and 3. (f) The amount of stretching,  $\beta$ , according to Model 1 and  $\rho_s = 2350 \text{ kg m}^{-3}$  and variable  $Z_{\text{neck}}$ . Heavy lined profile based on  $Z_{\text{neck}} = 7.2 \text{ km}$ . Fine lined profiles based on  $Z_{\text{neck}} = 5$  and  $10 \text{ km}$ . (g) Crustal model of the transition between oceanic and continental crust at the Gabon margin based on Model 1 and  $\rho_s = 2350 \text{ kg m}^{-3}$  and  $Z_{\text{neck}} = 7.2 \text{ km}$ . Dashed lines show the initial crustal configuration prior to sediment loading. Vertical dashed lines on (d)–(g) show the inferred mechanical boundaries at the margin.

the amplitude of the high while decreasing  $Z_{\text{neck}}$  increases it. Thus, differences in  $Z_{\text{neck}}$  have little influence on our conclusion of a weak zone. In contrast, changing the  $T_e$  structure during and after rifting (Fig. 5a) effects *both* the high and the seaward low. The main question is whether a weak zone is actually required by the data. Fig. 5a shows that decreasing the significance of the weak zone (i.e. Models 2 and 3) produces a high that is too wide in comparison to the observed. In addition, the seaward gradient of the high is displaced too far in a seaward direction. We conclude therefore that a weak zone *is* required by the stratigraphic and gravity anomaly data offshore Gabon and that changes in density,  $Z_{\text{neck}}$  and the  $T_e$  structure have little effect on the robustness of this conclusion.

## 6. Discussion

### 6.1. Mechanical thickness of extended continental lithosphere

A number of previous studies have suggested that the extended continental lithosphere that underlies rift-type basins in passive continental margins is relatively weak in comparison to that of normal oceanic and continental lithosphere. Most of these studies have been based, however, on the assumption that there was no flexural strength during rifting. We have tried to show here that even when the strength during rifting and depth of necking are taken into account, the best fit to the gravity anomaly at the Gabon margin is for a model in which a weak zone underlies a major part of the margin.

The proposed weak zone offshore Gabon is located just landward of a positive–negative magnetic anomaly ‘couple’ which Cande and Rabinowitz [20] interpret as the ocean–continent boundary. Furthermore, we know that oceanic lithosphere is not generally weak, except at the mid-oceanic ridge crest [27]. We conclude therefore that the weak zone offshore Gabon reflects the long-term thermal and mechanical behaviour of extended continental lithosphere.

The sediment backstrip and gravity anomaly have been modelled assuming that at least a portion of the extended continental lithosphere at the Gabon margin was weak during the post-rift sedimentation

phase. The lithosphere may also have been weak during rifting. At present, we do not understand why extended continental lithosphere would exhibit such a behaviour on long time-scales. There is good evidence, for example, that oceanic lithosphere recovers its strength as it cools and moves away from a mid-ocean ridge crest. We also know that as oceanic lithosphere cools, a progressively higher proportion of the support of long-term loads is achieved by the sub-crustal mantle. In the case of continental margins, most  $T_c$  estimates correspond to depths *within* the crust suggesting that the mantle is not often involved in the support of sediment loads. This may be the consequence of *either* a catastrophic reduction in the strength of the mantle during rifting *or* a mantle that is able to recover its strength following rifting but, is somehow mechanically decoupled from the strong overlying crust [28].

As a number of workers have pointed out [29–31], the strength of extended lithosphere has important implications for the structure of orogenic belts which develop on the sites of former passive margins and may ‘inherit’ their thermal and mechanical properties. Watts [31], for example, has suggested that the presence of weak zones may explain the extreme narrowness and great depth of some foreland basins which develop on the flanks of migrating thrust and fold loads. Wider basins may reflect the migration of these loads over the weak zone and onto the more rigid cratonic interiors. Other features of the weak zone crust may also be inherited during orogeny. For example, offshore Gabon, the weak zone is associated with  $\sim 15$  km thick crust, which is thicker than adjacent oceanic crust and extended continental crust. Such a thick crust would be more difficult to subduct and we speculate that these regions of weak, extended continental lithosphere, are capable of re-appearing as accreted terrains in orogenic belts.

## 6.2. Segmentation

Gravity anomaly maps (e.g. Fig. 1b) show that the low that flanks the edge effect high offshore Gabon extends for some 350–400 km *along-strike* of the continental slope. The low is abruptly terminated to the northwest at latitude 2°S by a belt of positive gravity anomalies. The anomalies extend from the continental shelf-break, across the slope, to

Sao Tomé; one of a number of small oceanic islands that comprise the Cameroon volcanic line. The low extends southeastwards to latitude 5.5°S where it is again terminated by a belt of positive anomalies. The positive anomalies correlate with a part of the margin offshore Angola where the slope appears to have prograded some tens of km more seaward than adjacent parts of the margin. The positive anomalies continue southeastwards to about latitude 8°S where they are replaced once more by negative anomalies.

These observations suggest that there is a distinct ‘gravity segmentation’ of the West Africa margin. We recognise (e.g. Fig. 1b) three such segments offshore Gabon, Congo and Angola. The long-term mechanical properties of the lithosphere beneath Segment 1 has been the principal focus of this paper. The presence of a wide belt of high-amplitude positive anomalies over Segment 2 suggests (e.g. Fig. 2) that the sediments there may have loaded lithosphere which has a relative high  $T_c$ . Segment 3 correlates with a narrow high and wide flanking low which resembles the patterns of Segment 1. This may indicate the return of a weak zone beneath this segment.

Unfortunately, these conclusions concerning the long-term mechanical properties of the lithosphere that underlie Segments 2 and 3 are speculative and need to be verified by backstripping and gravity modelling studies, once stratigraphic data from these regions become available. The patterns of anomalies are suggestive, however, of major changes in lithospheric strength at latitude 5.5°S and 8°S. Furthermore, satellite-derived gravity anomalies [32] show the conjugate margin of northeast Brazil to be segmented. The intense gravity ‘low’ associated with the Jacuibe basin, for example, is terminated at latitude 11°S and 13°S by more positive anomalies. Therefore, major changes in lithospheric strength may also occur along Gabon’s conjugate margin. If these inferences are correct, then it suggests that despite their morphological linearity passive continental margins may be highly segmented as regards their long-term strength.

## 6.3. Modes of extension

The model that best explains the sediment backstrip and gravity anomaly data (i.e. the heavy solid

line in Fig. 5f) suggests that  $\beta$  increases from  $\sim 1$  over the unstretched continental crust to  $\sim 4$  over the oceanic crust. The peak value of  $\beta \sim 5$  occurs, however, a few km seaward of the continental shelf-break. This is some 140 km *landward* of the oceanic–continent boundary inferred from seismic and magnetic anomaly data, suggesting that the locus of maximum thinning of the crust does not occur near this boundary but, several tens of km landward of it. Such an observation is in agreement with the results of numerical modelling [33] which show that when strain hardening occurs during the cooling of initially warmer lithosphere, the main locus of thinning shifts from the ocean–continent boundary and into the continent.

As Fig. 5f shows,  $\beta$  depends on the parameter  $Z_{\text{neck}}$ . At the Gabon margin, the dependency is most clearly seen in the thinned zone where  $Z_{\text{neck}}$  values of 5, 7.2 and 10 km yield average  $\beta$  values of 3, 4 and  $>6$  respectively. We have been able to rule out values of  $Z_{\text{neck}}$  of 5 and 10 km because they predict gravity anomalies which are either too low or too high in amplitude to explain the observed anomalies. The best overall fit is for  $Z_{\text{neck}} = 7.2$  km and, hence, we conclude that the best fit average  $\beta$  in the thinned zone is about 4.

It should be apparent from Fig. 5 that the  $\beta$  deduced from backstripping and gravity modelling will not necessarily be the same as deduced by studies which rely, for example, only on fitting thermal models to backstripped well data. They will agree in the special cases that: (a)  $Z_{\text{neck}} = 7.2$  km since this depth of necking predicts an Airy-type response, irrespective of the actual  $T_e$  during the rifting; and (b)  $T_e = 0$  km during rifting. They will also agree *if* the well data are backstripped taking into account the appropriate  $Z_{\text{neck}}$  and  $T_e$  during rifting. If these parameters are not known then it is necessary to first constrain them by gravity modelling. It is not sufficient, we believe, to justify the use of an Airy model in backstripping simply by noting, as some workers have done, that the free-air gravity anomalies over a region are of small-amplitude. The gravity anomalies have actually to be modelled because as Fig. 4 clearly shows, small-amplitude sum anomalies may, in some cases, be produced by high values of  $Z_{\text{neck}}$  and  $T_e$  during rifting.

Finally, our technique has implications for the ex-

ploration of deep-water passive margins, especially by the hydrocarbons industry. Seismic data provide important constraints on the physical properties of the crust. However, in many situations these data fail to unambiguously constrain the spatial distribution of extended continental lithosphere. The method used in this paper is based on observations that extended continental lithosphere may respond in fundamentally different ways to rifting and sediment loading than oceanic lithosphere. Further backstripping and gravity modelling studies which use 3-D 'grids' of sediment thickness and high-resolution satellite-derived gravity anomaly data, together with the development of more refined models, have the most promise, we believe, in better understanding the distribution, thickness and, rheology of extended continental lithosphere in the future.

## 7. Conclusions

The following conclusions can be drawn from this study:

(1) The amount of crustal thinning,  $\beta$ , beneath a rift-type basin can be determined *directly* from sediment backstrip data even in cases where there are believed to be variations in the strength and depth of necking during rifting.

(2) The model that best explains free-air gravity anomaly data offshore Gabon is one in which the continental slope is underlain by a 120 km wide zone which was mechanically weak after rifting and may have been weak during rifting.

(3) Magnetic anomaly and seismic reflection profile data suggest that the weak zone is mainly underlain by extended continental crust.

(4) Although the weak zone is associated with thinner than normal continental crust, the region of thinnest crust (i.e. highest  $\beta$  values) occurs *landward* of the weak zone, suggesting that the locus of maximum extension does not occur at the ocean–continent boundary but, is shifted some 100 km into the continent.

(5) Gravity anomaly maps suggest that the weak zone extends for some 350–400 km along-strike of the margin offshore Gabon. However, the West Africa margin as a whole appears to be highly segmented as regards its long-term strength.

## Acknowledgements

We are grateful to Alan Edwards of Fairway Geophysical for his stratigraphic interpretation of seismic reflection profile GWA88. This work was supported by a NERC ROPA award GR3/R9528 to ABW and a NERC studentship GT4/94/233/G to JS. [AC]

## References

- [1] S.J. Horsefield, R.B. Whitmarsh, R.S. White, J.-C. Sibuet, Crustal Structure of the Goban Spur rifted continental margin, NE Atlantic, *Geophys. J. Int.* 119 (1993) 1–19.
- [2] O. Eldholm, J. Skogseid, S. Planke, T.P. Gladchenko, Volcanic margin concepts, in: E. Banda, M. Torné, M. Talwani (Eds.), *Rifted Ocean–Continent Boundaries*, Vol. NATO ASI Series, Kluwer, Dordrecht, 1995, pp. 1–16.
- [3] A.B. Watts, W.B.F. Ryan, Flexure of the lithosphere and continental margin basins, *Tectonophysics* 36 (1976) 25–44.
- [4] A.B. Watts, Gravity anomalies, crustal structure and flexure of the lithosphere at the Baltimore Canyon Trough, *Earth Planet. Sci. Lett.* 89 (1988) 221–238.
- [5] S. Fowler, D. McKenzie, Gravity studies of the Rockall and Exmouth Plateaux using SEASAT, *Basin Res.* 2 (1989) 27–34.
- [6] W.E. Holt, T.A. Stern, Sediment loading on the western platform of the New Zealand continent: implications for the strength of a continental margin, *Earth Planet. Sci. Lett.* 107 (1991) 523–538.
- [7] H. Kooi, S. Cloetingh, J. Burrus, Lithospheric necking and regional isostasy at extensional basins, 1. Subsidence and gravity modeling with an application to the Gulf of Lions margin (SE France), *J. Geophys. Res.* 97 (1992) 17553–17571.
- [8] G. Spadini, S. Cloetingh, G. Berlotti, Thermo-mechanical modeling of the Tyrrhenian Sea, *Tectonics* 14 (1995) 629–644.
- [9] A.B. Watts, C. Marr, Gravity anomalies and the thermal and mechanical structure of rifted continental margins, in: E. Banda, M. Talwani, M. Torné (Eds.), *Rifted Ocean–Continent Boundaries*, Kluwer, Dordrecht, 1995, pp. 65–94.
- [10] J. Braun, C. Beamont, Styles of continental rifting: results from dynamic models of lithospheric extension, in: C. Beamont, A.J. Tankard (Eds.), *Sedimentary Basins and Basin-Forming Mechanisms*, *Can. Soc. Pet. Geol.* 12 (1987) 241–258.
- [11] C. Goetze, B. Evans, Stress and temperature in the bending lithosphere as constrained by experimental rock mechanics, *Geophys. J. R. Astron. Soc.* 59 (1979) 463–478.
- [12] G. Bertotti, M. ter Voorde, S. Cloetingh, V. Picotti, Thermo-mechanical evolution of the South Alpine rifted margin (North Italy): constraints on the strength of passive continental margins, *Earth Planet. Sci. Lett.* 146 (1997) 181–193.
- [13] J.K. Weissel, G.D. Karner, Flexural uplift of rift flanks due to mechanical unloading of the lithosphere during extension, *J. Geophys. Res.* 94 (1989) 13919–13950.
- [14] C.E. Keen, S.A. Dehler, Extensional styles and gravity anomalies at rifted continental margins: some North Atlantic examples, *Tectonics* 16 (1997) 744–754.
- [15] P.D. Rabinowitz, Gravity measurements bordering passive continental margins, in: R.A. Scrutton (Ed.), *Dynamics of Passive Margins*, vol. 6, Am. Geophys. Union, Washington, 1982, pp. 91–115.
- [16] P.D. Rabinowitz, J. LaBrecque, The Mesozoic South Atlantic Ocean and evolution of its continental margins, *J. Geophys. Res.* 84 (1979) 5973–6002.
- [17] P. Teisserenc, J. Villemin, Sedimentary basin of Gabon — geology and oil systems, in: J.D. Edwards, P.A. Santogrossi (Eds.), *Divergent/Passive Margin Basins*, Am. Assoc. Pet. Geol. 48 (1989) 117–199.
- [18] L.P. Magnavita, I. Davison, N.J. Kusznir, Rifting, erosion, and uplift history of the Reconcavo–Tucano–Jatobá Rift, northeast Brazil, *Tectonics* 13 (1994) 367–388.
- [19] J.B. Meyers, B.R. Rosendahl, J.A. Austin, Deep-penetrating MCS images of the South Gabon Basin: implications for rift tectonics and post-breakup salt remobilization, *Basin Res.* 8 (1996) 65–84.
- [20] S. Cande, P. Rabinowitz, Mesozoic seafloor spreading bordering conjugate continental margins of Angola and Brazil, 10th Offshore Technology Conf. Proc. 3 (1978) 1869–1876.
- [21] G.D. Karner, M.S. Steckler, J. Thorne, Long-term mechanical properties of the continental lithosphere, *Nature* 304 (1983) 250–253.
- [22] P.J. Barton, R.J. Wood, Tectonic evolution of the North Sea Basin: Crustal stretching and subsidence, *Geophys. J. R. Astron. Soc.* 79 (1984) 98–1022.
- [23] C.J. Ebinger, G.D. Karner, J.K. Weissel, Mechanical strength of extended continental lithosphere: Constraints from the western rift system, *Tectonics* 10 (1991) 1239–1256.
- [24] P.R. Vail, R.M. Mitchum, S. Thompson, Relative sea-level from coastal onlap, in: C.E. Payton (Ed.), *Seismic Stratigraphy — Applications to Hydrocarbon exploration*, Am. Assoc. Pet. Geol. Mem. 26 (1977) 63–82.
- [25] J.H. Bodine, M.S. Steckler, A.B. Watts, Observations of flexure and the rheology of the oceanic lithosphere, *J. Geophys. Res.* 86 (1981) 3695–3707.
- [26] J. Stewart, Gravity anomalies and Lithospheric flexure: Implications for the thermo-mechanical evolution of the continental lithosphere. Ph.D thesis, University of Oxford, 1998.
- [27] J.R. Cochran, An analysis of isostasy in the world's oceans, 2. Midocean ridge crests, *J. Geophys. Res.* 84 (1979) 4713–4729.
- [28] E.B. Burov, M. Diament, The effective elastic thickness ( $T_e$ ) of continental lithosphere: What does it really mean? *J. Geophys. Res.* 100 (1995) 3895–3904.

- [29] G.S. Stockmal, C. Beaumont, R. Boutilier, Geodynamic models of convergent margin tectonics: transition from rifted margin to overthrust belt and consequences for foreland-basin development, *Am. Assoc. Pet. Geol.* 70 (1986) 181–190.
- [30] P. Desegaulx, H. Kooi, S. Cloetingh, Consequences of foreland basin development on thinned continental lithosphere: application to the Aquitaine basin (SW France), *Earth Planet. Sci. Lett.* 106 (1991) 116–132.
- [31] A.B. Watts, The effective elastic thickness of the lithosphere and the evolution of foreland basins, *Basin Res.* 4 (1992) 169–178.
- [32] D.T. Sandwell, W.H.F. Smith, Marine gravity anomaly from Geosat and ERS-1 satellite altimetry, *J. Geophys. Res.* 102 (1997) 10039–10054.
- [33] G. Bassi, C.E. Keen, P. Potter, Contrasting styles of rifting: Models and examples from the eastern Canadian margin, *Tectonics* 12 (1993) 639–655.
- [34] J.D. Fairhead, A.B. Watts, P. Chevalier, B. El-Haddeh, C.M. Green, G.W. Stuart, K.A. Whaler, I. Windle, African Gravity Project, GETECH, Department of Earth Sciences, University of Leeds, 1988.